Extracellular Pax6 regulates tangential Cajal-Retzius cell migration

H. Kaddour[a,b,c], E. Coppola[b], A. Di Nardo [a], A. Wizenmann[d], M. Volovitch[a], A. Prochiantz[a] and A. Pierani[b,c]

(a) CIRB, CNRS UMR 7241 / INSERM U1050, Collège de France, 11 place Marcelin Berthelot, 75231 Paris, France

(b) Institut Jacques Monod, CNRS UMR 7592, Université Paris Diderot, Sorbonne Paris Cité, 15 rue Hélène Brion, 75013 Paris, France.

(c) Imagine Institute and Center of Psychiatry and Neuroscience, Université Paris Descartes, 102-108 rue de la Santé, 75014 Paris, France (present adress)

(d) Department of Anatomy, Institute of Clinical Anatomy and Cell, University of Tübingen, Osterbergstrasse 3, 72074 Tübingen, Germany.

Running Title: Tangential migration in the developing cortex is controlled by extracellular Pax6

Keywords: Pax6, non-cell autonomous, Cajal-Retzius neurons, migration, embryonic cerebral cortex

Abstract

The embryonic mouse cortex displays a striking low caudo-medial and high rostro-lateral graded expression of the homeoprotein transcription factor Pax6, which presents both cell autonomous and direct non-cell autonomous activities. Through the genetic induction of anti-Pax6 single-chain antibody secretion, we have analyzed Pax6 non-cell autonomous activity on the migration of cortical hem- and septum-derived Cajal-Retzius (CR) neurons by live imaging of flat mount cerebral cortices. We observed that blocking extracellular Pax6 disrupts tangential CR cell migration patterns in the developing cerebral cortex. We found both a decrease in the distance travelled and the directionality in addition to changes in the depth at which they migrate. Tracking of single CR cells in mutant cortices revealed that contact repulsion was enhanced in medial and reduced in lateral regions. In vitro studies suggest that extracellular Pax6 could control neuronal migration patterns by direct/or indirect modulation of signaling cascade components involving EphrinA3. This study highlights for the first time that Pax6 non-cell autonomous activity controls neuronal migration.

Introduction

Glutamatergic Cajal-Retzius cells (CR cells) are a transient neuron population residing at the surface of the developing cerebral cortex (Marin-Padilla, 1998). They comprise molecularly distinct subtypes born in three different progenitor domains of the mouse cortical neuroepithelium: the cortical hem (CH), the septum (S) and the ventral pallium at pallial-subpallial boundary (Bielle et al., 2005; Yoshida et al., 2006; Tissir et al., 2009). Between embryonic days 10.5 (E10.5) and 12.5, CR cells migrate tangentially within the preplate to specifically populate the caudo-medial, rostro-medial and lateral cortex (Bielle et al., 2005; Griveau et al., 2010; Villar-Cervino et al., 2013a). CR cell migration and distribution at the surface of the neocortex play important roles in controlling the size and positioning of primary and higher-order cortical areas (Griveau et al., 2010; Barber et al., 2015). It has been proposed that CR cells act as mobile signaling cells that participate in the production and maintenance of morphogen gradients required to coordinate neurogenesis and to delineate areal boundaries within the cortical ventricular zone (VZ)(Griveau et al., 2010).

At the molecular level, transcription factors play key functions in the early regionalization of the cortex (Brunet et al., 2007; O'Leary et al., 2007). Among them, the homeoprotein (HP) family has been the focus of several theoretical and experimental studies showing that they play essential function in the positioning of boundaries within the developing cortex and, beyond, in the entire nervous system. In particular, the role of Pax6 and Emx2 was demonstrated in the positioning of the boundary between the primary visual and somato-sensory territories (O'Leary et al., 2007; Prochiantz and Di Nardo, 2015; Ypsilanti and Rubenstein, 2016). A link between Pax6 and the control of CR cell migration was suggested by previous studies where accumulation of CR cells in the rostral pallium (Matsuo et al., 1993; Stoykova et al., 2003) and abnormal migration of CH-CR cells was detected in Sey mutant embryos (Ceci et al., 2010). Up to date, the role of HDs in early cortical regionalization is thought to be through intrinsic mechanisms in progenitor cells. However, many HPs, including Pax6, were shown to be secreted and internalized (Prochiantz, 2000; Joliot and Prochiantz, 2004) and thus to display a non-cell autonomous function. Pax6 was found at the cell surface of ventral neural tube tissues where it regulates the migration of oligodendrocyte precursors (Di Lullo et al., 2011) and the graded expression of extracellular Engrailed, another HP, is a guidance cue for retinal growth cones navigating at the surface of the optic tectum (Brunet et al., 2005). We therefore investigated whether Pax6 regulates CR

cell migration via a cell autonomous or non-cell autonomous activity. To specifically trigger removal of extracellular Pax6 we used a mouse model harboring the sequence for inducible single-chain antibody (scFv) directed against Pax6 in the ROSA26 locus (Bernard et al., 2016). In this study, we demonstrate that neutralizing Pax6 in the extracellular space modifies the migration characteristics and behaviors of CH- and S-CR cells.

Results

Following CR trajectories in 4 dimensions

By imaging E11.5 flattened cortices in culture, we specifically followed CR cells generated at the level of the CH and septum (CH-CR cells and S-CR cells, respectively) using the *ΔNp73*^{Cre} mouse line in which Cre and EGFP are specifically expressed in these two cell populations (Tissir et al., 2009) (Fig. 1A). To compare CR migration in a wild-type environment or upon Pax6 extracellular neutralization (thereafter, mutant), scFvPax6 single chain secreted anti-Pax6 antibody was induced by crossing *ΔNp73*^{Cre} and *scFvPax6* mouse lines (Tissir et al., 2009; Bernard et al., 2016). The Pax6 scFv was characterized in earlier studies (Lesaffre et al., 2007; Di Lullo et al., 2011; Bernard et al., 2016). It is specific for Pax6 and devoid of a significant cell-autonomous activity, even when expressed without signal peptides, likely because of the instability of disulfide bonds in the reducing cytoplasmic milieu (Lesaffre et al., 2007).

Four cortices were used for each genotype (wild type and mutant) allowing the tracking of more than 700 CR cells during 8 hrs to obtain 4D views of cell migration (Fig. 1A,B). Initial cell positions were not exactly the same in each cortex, reflecting slightly different embryonic stages (Fig. 1b). Indeed, development proceeds very rapidly and CR cells generated between E10.5 to E11.0 cover the entire pallium within 12 hrs (Bielle et al., 2005; Griveau et al., 2010). Explants with higher number of tracks medially represent younger stages when migration has just started at sites of origin. Inter-cortical heterogeneity in cell position was observed in control and mutant cortices, at the onset and end of filming. We, thus, reasoned that if the effect of blocking extracellular Pax6 is robust enough, it will be visible regardless of this heterogeneity and first performed a global analysis before subdividing cortices into several compartments.

Extracellular Pax6 influences CR cell migration trajectories

To compare CR cell subtypes in the different cortices, we imposed a theoretical migration starting point for all cells in order to analyze each cortex separately (Fig. 2A, B) and to pool the data for each condition (Fig. 2C). We first qualitatively confirmed that cell viability was preserved during the 8 hrs of image acquisition by following the progression of migration during 4 successive time intervals in pool cortices (Fig. S1A). In control conditions

for both CR cell subtypes, track path length increased progressively suggesting that cell migration globally continues up to the end of the imaging period. For S-CR cells in mutants, tracks were shorter from the beginning to the end of migration indicating that neurons seemed to cover lower distance than in control conditions. In contrast, tracks of CH-CR cells in mutants evolved similarly to those in controls (Fig. S1A). Furthermore, for both CR cell subtypes, the mean speed after 480 min of recording showed no differences between control and mutant cells suggesting that blocking extracellular Pax6 did not affect their ability to migrate (Fig. S1B). The progressive increase in track length and the maintenance of an average speed over time demonstrate that neurons are viable in flattened cortices during the imaging period.

We next analyzed the migration pattern of CR cells after 480 min of recording, in each separate cortex (Fig. 2A) and pooled cortices (Fig. 2B) by quantifying the trajectories along the medio-lateral and the rostro-caudal axis (Fig. 2B). Compared to controls, both mutant S- and CH-CR cells presented shorter track path length with a lower directionality index indicating that mutant CR neurons migrate along less linear trajectories (Fig. 2A-C). The majority of S- and CH-CR cells in controls migrated towards lateral regions with a preference for the rostro-lateral (*rl*) direction (35.6% and 51.3 %, respectively) (Fig. 2B). In mutants compared to controls the percentage of S-CR cells migrating towards *rl* territories increased (45.5% *vs* 35.6%, respectively) (Fig. 2B) whereas that of CH-CR cells migrating caudo-laterally (*cl*) was preferentially enhanced (35.4% *vs* 21.1%, respectively) (Fig. 2B). To further examine these differences, we analyzed distances travelled by CR cells focusing on lateral directions (Fig. 2D, E). Extracellular Pax6 neutralization was efficient in decreasing path length of S-CR cells migrating rostro-laterally (39.73%) as well as Euclidean distance, although with a smaller but significant effect (21.61%). Notably, no differences were observed for S-CR cells migrating caudo-laterally. For CH-CR cells, Pax6 neutralization resulted in a reduction of both path length and Euclidean distance values whether they migrated *rl* or *cl* (25.59% *vs* 41.82% and 15.34% *vs* 32.02%, respectively). A representative trajectory of CR cells in each condition (Fig. 2D, E) illustrates that neutralizing Pax6 modifies the migration of S-CR and CH-CR neurons toward the lateral part of the developing cortex with a stronger decrease in overall Euclidean distance than total path length. Together these results suggest that Pax6 influences more strongly directionality than total path length, thus the ability to migrate.

Position-dependency of non-cell autonomous Pax6 activity

To study whether the effect of extracellular Pax6 neutralization depended on the region of the developing cortex where CR cells migrated, we took into account the differences in CR cell tracking start positions. Cortices were subdivided into 4 compartments along the medio-lateral and the rostro-caudal axis with a number of cells ranging from 97 to 265 per compartment, numbers allowing statistical analyses. The two rostral territories (RM and RL) are enriched in S-CR cells, while the caudal ones (CM and CL) primarily contain CH-CR cells. In addition, RM and CM compartments are closer to the CR cell sources than RL and CL compartments which abut the "arrival regions". CR migration was analyzed separately for the 4 compartments (Fig. 3A-D). In all 4 compartments both S- and CH-CR cells in mutants traveled shorter Euclidean distances along the medio-lateral axis with respect to controls. However, along the rostro-caudal axis migration of both CR subtypes was only influenced by Pax6 neutralization in the lateral compartments where both S- and CH-CR cells appeared to travel shorter euclidean distances and to move less along the rostro-caudal axis (Fig. 3C, D). The mean directionality vectors of controls and mutants (Fig. 3E) summarize the effect of blocking extracellular Pax6 on trajectories in the different territories. It shows that distances traveled are reduced for mutant CR cells in all 4 compartments while the direction of migration is more highly affected in the lateral cortex with an overall increase of migration in the rostral direction at the expenses of that towards caudal regions. Taken together, these results show that neutralization of extracellular Pax6 reduces the distance traveled by CR cells leaving their medial origins as well as when reaching the end of migration in the lateral cortex. Notably, they also indicate that in the lateral compartments, where the Pax6 concentration is higher rostrally, the neutralization of its extracellular activity redirects the cells in the rostral direction, suggesting a repelling activity of high extracellular Pax6 concentration.

Blocking extracellular Pax6 affects the depth of CR cell migration

Previous studies have analyzed migration parameters of CR cells in 2-D or 3-D environments (Villar-Cervino et al., 2013a; Barber et al., 2015). Migration along the depth of the tissue was not previously analyzed in whole-flatted cortical preparations because of the very big size of the movies. We devised a method to analyzed over 15 Go timelapse files by movie frame separation and reconstruction (see Methods). We were, thus, able to analyze the

effect of Pax6 neutralization on S- and CH-CR localization within the depth (Z axis) of the developing cortex as a function of time and in the 4 compartments of interest (Fig. 4). Our data demonstrate that close to CR sources (RM and CM domains), S- and CH-CR cells migrated at 40% or 30% depth respectively, with a wider dispersion between the ventricular side and the pial surface in the mutants, an effect particularly marked for CH-CR cells (Fig. 4A). Percentages along the Z-axis might not represent real values as in vivo considering that the ventricular zone shrinks in flattened cortex cultures. When close to the end of their migration zone (RL and CL territories), CH-CRs in controls appeared to spread highly along the depth compared to S-CRs which migrated at about 50% depth. This behavior was lost in the mutant environment where both S-CR and CH-CR cells migrated very close to the pial surface (Fig. 4B). Representative images of the different regions of interest are shown in Figure 4A, B demonstrating that blocking extracellular Pax6 strongly changes the distribution of CR neurons along the depth of the developing cortex.

Non-cell autonomous effects on CR cell contact repulsion

CR cells, in particular CH-CR cells, were shown to tangentially invade the developing cortex by contact-repulsion. This was defined as when the growth cone of a CR cell comes into contact with another CR cell its leading process retracts, the direction of migration changes with an angle of more than 90°, and migration speed increases (Villar-Cervino et al., 2013a). In support of contact-repulsion, we found that CR cell migrate faster at the onset of migration when cell density is higher and, in particular, CH-CR cells displayed enhanced migration speed upon neutralization of extracellular Pax6 (Fig. S2A, B). After 1hr of recording, the speed was reduced for both CR cell subtypes with lower values recorded in mutants (Fig. S2A, B) suggesting that blocking extracellular Pax6 may have contrasted effects at the onset and at the end of migration.

We therefore tested whether changes in contact-repulsion may be involved in the migration defects observed in mutants (Fig. 5). GFP^+ CR cells were clustered into two groups depending on whether or not they encounter and contact another GFP^+ CR cell during migration (Fig. 5A). In control conditions, S- and CH-CR cells behaved differently, as CH-CR cells displayed higher number of contacts in medial and lateral domains compared to S-CR cells (74% in CL and 71% in CM *vs* 64% in RM and 56% in RL). Blocking extracellular Pax6 increased contacts between S-CR cells in the RL domain (73% *vs* 64%) and, on the contrary, decreased contacts in CH-CR cells in both CM and CL territories (Fig. 5A). To gain

a better insight into these differences, we further separated cells initiating contacts in two groups (Fig. 5B-D): *(i)* contact-repulsion (Fig. 5B); and *(ii)* contact-without-repulsion when following contact the cells remain in contact longer and do not change their direction of migration (Fig. 5C). In control conditions, a higher percentage of both CR cell subtypes showed contact-repulsion in medial than in lateral domains confirming previous results that contact-repulsion could be an important mechanism for cells dispersion from their sources (Villar-Cervino et al., 2013b). Blocking extracellular Pax6 enhanced contact-repulsion in medial regions and significantly diminished it in lateral regions (Fig. 5D). These differences were more marked for CH-CR cells suggesting that neutralization of Pax6 is more efficient in caudal regions.

Pax6 mediated contact-repulsion of CR cells through Ephrin-A3

At the molecular level, contact-repulsion of CR cells was shown to be mediated by Eph receptors and their membrane-bound Ephrin ligands. Abrogating Eph/ephrin signaling in CH-CR cells *in vitro* by adding Ephrin-A3 was shown to reduce contact-repulsion and to increase the time during which CR cells remained in contact (Villar-Cervino et al., 2013b). Moreover, Pax6 was shown to control olfactory cortex neurons migration through modulation of Ephrin-A5 expression (Nomura et al., 2006). To test if secreted Pax6 could control this signaling pathway in CR cells, we performed protein stripe assays in which dissociated hem explants were cultured on alternating Ephrin-A3- and laminin-containing lanes (Figure 6). In control conditions, the presence of Ephrin-A3 increased the percentage of CH-CR cells in the ephrin stripes compared with laminin stripes. Blocking extracellular Pax6 further accentuated this effect (63.4%) (Fig. 6 A, B), suggesting that secreted Pax6 could modulate Ephrin-A3 effect on CR adhesive behavior and possibly migration.

Discussion

In this study we used a genetic strategy to trigger the expression and secretion of a single chain antibody against Pax6 and neutralize extracellular Pax6 in the developing cortex in order to study the non cell autonomous function of this transcription factor during neuronal migration (Prochiantz and Di Nardo, 2015; Bernard et al., 2016). We show that neutralizing secreted Pax6 modifies the tangential trajectories and migratory behaviors of S- and CH-CR cells.

Understanding the mechanisms which control correct positioning of CR neurons at the cortical surface is a crucial issue since perturbing CR subtypes distribution and migration alters the position and size of primary (Griveau et al., 2010) and higher-order areas (Barber et al., 2015). Using live imaging and genetic labeling, we followed S- and CH-CR cells during early phases of migration. Upon extracellular Pax6 neutralization, we observed similarities and differences in the responses of the two subtypes analyzed. In terms of path length and Euclidian distances, neutralizing Pax6 had a negative effect, although stronger on Euclidian distance, both on S-CR and CH-CR cells migrating with a rostro-lateral direction towards the high concentration of Pax6 gradient expression. Notably, this had no effect on S-CR cells whose tracks were oriented along the caudo-lateral direction away from the high Pax6 concentration. In terms of directionality, S-CR and CH-CR cells responded similarly with a strong tendency to migrate more rostro-laterally in the mutant, an effect particularly striking for S-CR cells in the lateral region where Pax6 expression is higher. Together these results suggest a repulsive activity of high extracellular Pax6 concentration in the lateral most regions. Furthermore, for both subtypes the stronger effect of Pax6 neutralization on Euclidian distance than on path length and a reduction in directionality index is in favor of a disorganization of migration with little effects on the ability to migrate, as further supported by the absence of changes in average speed (Figure S1). Wild-type CH-CR cells were previously found to migrate by expanded routes in Sey mutants embryos, in which both intracellular and extracellular Pax6 are eliminated, compared to control embryos (Ceci et al., 2010). They appeared to travel longer distances and to disperse more broadly along the rostro-caudal and Z axis. Interestingly, we observed that CR cells of both subtypes travelled shorter distances and dispersed less on both the RC and Z axis upon specific removal of extracellular Pax6. Although timelapse microscopy was not perfomed in the Ceci et al. report, together these data suggest a specific function of extracellular Pax6 on CR cell migration.

Furthermore, we found that the effect on CR cell directionality upon neutralization of secreted Pax6 depends on cell position at the onset of recording and global direction along the rostro-caudal axis is more highly disturbed in lateral regions correlating with high levels of Pax6 expression. As extracellular Pax6 is cleared in S- and CH-specific mutants with a medial to lateral gradient due to the migration of CR subtypes from their sources at E11.5, our results not only argues in favor of an even stronger effect on CR migration if Pax6 would have been eliminated with a rostro-lateral high gradient, but also for the first time of a dose- and region-dependent effect of Pax6 in neuronal migration. Indeed, the analysis of CR cell dispersion within the neuroepithelium (Z axis) indicated some differences in the effect of Pax6 neutralization between S-CR and CH-CR cells and also between territories. In the medial compartments (RM and CM), neutralizing Pax6 had little influence on migration in the Z axis, although a wider dispersion was noticed for CH-CR cells in the mutant (Figure 4). In the lateral compartments, both S-CR and CH-CR cells migrated closer to the surface in the mutant than in the wild type. This effect was milder for CH-CR cells since control cells navigated more randomly dispersed along the Z axis. It has been proposed that chemokines such as CXCL12 secreted by the meninges both enhance CR cell motility and maintains them close to the pial surface (Borrell and Marin, 2006). Our results thus suggest that, in as much as the Z axis is concerned, extracellular Pax6 and CXCL12 may have opposite effects on the migration of CR cells on the Z axis and on their maintenance in the marginal zone. Altogether, our findings show for the first time that extracellular Pax6 controls non-cell autonomously CR neuron migration, an observation reminding of the paracrine activity of Pax6 in oligodendrocyte precursor cell migration in the embryonic chick spinal cord (Di Lullo et al., 2011).

Contact-repulsion was shown to be an important mechanism by which CR cells populate the cortex at early stages. In live-imaging studies, CR cells are repelled upon contact with neighbor cells resulting in the collapse and retraction of their leading process and a change in their direction of migration (Villar-Cervino et al., 2013b; Barber et al., 2015). It was also shown that a proportion of neurons migrate and randomly change their direction without contacting adjacent cells (Villar-Cervino et al., 2013b). In the case of S-CR cells, neutralizing Pax6 increased the number of contacts in the RL but not in the RM compartment, although contacts were more often followed by repulsion in the latter compartment. In the case of CH-CR cells, they showed a decrease in the number of contacts in the CM and CL

with increased and decreased repulsion in the CM and CL compartments, respectively. These results suggest that there is no linear relationship between contact-repulsion and that the absence of extracellular Pax6 favors cell dispersion in the medial compartments, thus near CR cell sources. Eph/ephrin signaling was previously shown to be involved in contact-repulsion. Abrogating this pathway increased the time of CH-CR cell contact and their persistence in directionality, thus reducing their ability to undergo contact-repulsion (Villar-Cervino et al., 2013b). Here, we found that CH-CR cells from mutant CH explants displayed an enhanced preference for Ephrin-A3 stripes, suggesting that they display lower contact-repulsion and therefore Eph/ephrin signaling is decreased when extracellular Pax6 is neutralized. These data are in agreement with the increase in repulsion found in flattened cortices in the caudal-medial region, which corresponds to the origin of CH-CR cells used for *in vitro* assay. Together with the finding that in mutants, contacts between CH-CR cells are reduced, the increased repulsion probably due to altered signaling pathway can explain the migration defects we detected when extracellular Pax6 is neutralized.

Our findings raise the intriguing hypothesis that several mechanisms can be employed by a gene/protein to execute the same function. We suggest that Pax6 may control cortical arealization by directly acting as a transcription factor in neuronal progenitors and indirectly as a guidance factor for proper CR cell migration. Therefore, slight changes in the levels and distribution of extracellular Pax6 during brain development could have important consequences in physiopathology and be at the origin of evolutionary modifications in the mammalian cerebral cortex.

METHODS

Animals

scFvPax6 (Bernard et al., 2016) and *ΔNp73*^{CreIRESGFP}(Tissir et al., 2009) transgenic mice were kept in a C57BL/6J background. Animals were genotyped by PCR using specific primers for each allele. The day of vaginal plug was considered to be E0.5. All animal procedures, including housing, were carried out in accordance with the recommendations of the European Economic Community (86/609/EEC), the French National Committee (87/848) and French bylaws (AGRG1240332A / AGRG1238724A / AGRG1238767A / AGRG1238729A / AGRGR1238753A). All mouse work was approved by the Veterinary Services of Paris (Authorization number: 75-1454) and by the Animal Experimentation Ethical Committee Buffon (CEEA-40) (Reference: CEB-34-2012).

Whole Flattened Cortices Culture

Whole flattened cerebral cortices cultures were adapted from Barber M., *et al* 2015. Cortices were dissected from E11.5 *ΔNp73*$^{Cre/+}$ (control) and *ΔNp73*$^{Cre/+}$*;scFvPax6*$^{tg/o}$ (mutant) embryos. One single incision was made to remove the ventral subpallial tissue. Explants were cultured for 5 hours (hrs) before time lapse acquisition on a Millicell permeable membrane (pore size 0.4 µm; Millipore) with the ventricular side facing the membrane, in phenol-red-free high glucose DMEM (Sigma) containing B27 supplement (Gibco) and penicillin/streptomycin antibiotics (100 µg/ml, Sigma) in 5% CO_2 at 37°C. Shortly before imaging, the flattened cortex was transferred with the Millicell membrane and inverted onto a glass-bottom microscope imaging chamber with the pial surface directly adjacent to the glass. Explants were mounted in purified bovine collagen gel (25µl/explant, Advanced Biomatrix), which polymerizes in 15 min at 37°C.

4D time-lapse acquisition

Time lapse acquisition of migrating CR cells was performed over 8 hrs in an incubation chamber at 37°C and 5% CO_2 containing phenol red-free DMEM solution and using an inverted laser scanning confocal microscope (Zeiss 780) with an oil immersion 25x objective. EGFP protein excited at 488 nm and images were acquired at 500-550 nm. Depending on explant size, 4D time-lapse images were generated by acquiring automatically 9-14 optical Z

sections with a z-step size of 8 µm every 30 min and 70-140 focal tiles were merged to visualize the entire flattened cortex with a 512 × 512 pixel resolution.

Bioinformatics Processing and movies analysis

Successive steps were used to disassemble and divide resulting movies, exceeding 15 GB, in time and Z points using successively the Zeiss Zen software (Carl Zeiss MicroImaging) and the ImageJ software to convert images in 3D tiff-stacks. 4D reconstruction and display of CR cell migration were built up by Imaris software (Bitplane, version 8.2.1). GFP^+ cell tracks were obtained from four flattened brains per phenotype (control or mutant). Using the spot cell-tracking module, cells were spatially classified depending on their genotype and origins (CH or S) and tracked manually over time and along the medio-lateral, rostro-caudal and depth axes. We selected CR cells migrating in the caudal quadrant of the explant as corresponding to CH-CRs cells, and those migrating in the rostral quadrant as S-CR cells (according to (Barber et al., 2015)). We excluded from the analysis CRs migrating at middle levels along the rostro-caudal axis for which the origin could not be ascertained. 1478 tracks were analyzed, 726 control cells and 752 mutant cells. The directionality index was calculated by dividing the Euclidean distance (the shortest distance between the start and end position of a cell trajectory) by the actual path length followed by the cells during migration. The overall directionality in migration was determined for each regions of interest by automatic clustering of tracks to a common origin using the Imaris transpose tracks function. In Figure 3e, a mean displacement vector along the medio-lateral and rostro-caudal axis was calculated for each region and represented in a 2-d vectorial projection clustered at a common origin. CR cell behaviors at contacts were subdivided and analyzed based on previous strategies (Villar-Cervino et al., 2013b; Barber et al., 2015). Briefly, contacts between two cells were scored if occurring within a single optical slice from $\Delta Np73^{Cre/+}$ (control) and $\Delta Np73^{Cre/+};scFvPax6^{tg/o}$ (mutant) explants in the rostral and caudal regions. The angle of deviation was observed using the Imaris cell-tracking spot module and considered contact with repulsion if cells changed trajectory with an angle of more than 90°.

Ephrin A3 Stripe assay

Striped carpets of purified EphrinA3 were produced as described (Knoll et al., 2007) (Wizenmann et al., 2009). Briefly, alternating purified EphrinA3 (R&D systems, 10µg/ml) lanes were laid down on coverslips previously coated with poly-lysine. Alexa488 labeled anti-

human IgGs (Jackson laboratories, 1:200) were added to the EphrinA3 solution to allow for immunohistochemical identification. EphrinA3 and control stripes were further coated with laminin (20 mg/ml). Hem explants were dissected from control and mutant embryos at E12.5 and mechanically dissociated. Pre-labeled cells (DiAsP, Invitrogen, 10µl/ml) were plated on the striped coverslips and incubated in methylcellulose-containing Neurobasal medium for 48 hrs. Cells were classified and counted as occupying or not a stripe containing EphrinA3.

Statistics

Prism 6 software (GraphPad, version 6.01) was used for statistical analysis. When data followed a normal distribution, paired comparisons were analyzed with t test, whereas multiple comparisons were analyzed using ANOVA with post hoc Bonferroni correction. Data are presented as mean and SEM throughout the manuscript. $p < 0.05$ were considered significant.

Author Contributions

H.K. designed and performed most of the experiments, A.W. designed and participated in the stripe assays, M.V. and A.D.N. produced and validated the *scFvPax6* mouse line, E.C. helped analyzing the data. A.P. and A.P. supervised the project and analyzed data. H.K., E.C. A.D.N., A.P. and A.P. wrote the manuscript.

Acknowledgements

We thank the ImagoSeine facility, member of the France BioImaging infrastructure supported by the French National Research Agency (ANR-10-INSB-04, “Investments for the future”) for help with confocal microscopy and Imaris software. We thank the Buffon Animal facility, Animalliance and L. Vigier for technical assistance and animal care. F. Tissir for providing the $\Delta Np73^{CreIRESGFP}$ mouse line (Brussels, Belgium). F. Lam and V. Contremoulins for help with movie reconstruction. A. Pierani is a CNRS (Centre National de la Recherche Scientifique) Investigators and member Teams of the École des Neurosciences de Paris Ile-de-France (ENP), E.C. is a University Paris Diderot Lecturer. This work was supported by grants from the ANR-MOST bilateral accord (ANR-13-ISV2-0001) to A. Prochiantz and A. Pierani, ERC Advanced Grant HOMEOSIGN (339379) to A. Prochiantz, ANR (ANR-2011-BSV4-023-01; ANR-15-CE16-0003-01) and FRM («Equipe FRM DEQ20130326521») to A. Pierani. Authors have no conflicts of interest.

Figure Legends

Figure 1: 4D-acquisition of CR cell migration patterns

(A) Overview of the successive steps to record and analyze the migration of GFP^+ CR cells.

(B) Cell tracks from 8 hr live imaging of S- and CH-CR cells in ED 11.5 flattened cortices of *ΔNp73*^{CreIRESGFP} (control) and *ΔNp73*^{CreIRESGFP}*;scFvPax6* (mutant) embryos. Tracks are represented by displacement vectors. The CR cells (S or CH) for which origin could not be ascertained were excluded from the images and their localization were delimited by dashed lines. Scale bar: 100 µm

Figure 2: Non-cell autonomous activity of Pax6 on CR cell trajectories and directionality

(A, B) Tracks of migrating S- and CH-CR cells (A) in each control and mutant cortex after 480 min along the medial-lateral and rostro-caudal axes. The tracks are pooled in (B) and the distribution of tracks per quadrant is shown by percentage.

(C) Directionality index is the ratio of Euclidean distance to path length trajectory distance.

(D, E) Path length and Euclidean distance travelled by CR cells in the RL and CL quadrants. Representative trajectories of S- and CH-CRs was illustrated in each condition. Scale bar : 10 µm.

Values are mean ± SEM; Anova test *ns*, not statistically different, $^{**}p < 0.01$, $^{***}p < 0.001$. CL: caudo-lateral; CM: caudo-medial; RL: rostro-lateral; RM: rostro-medial.

Figure 3: Position-dependency of non-cell autonomous Pax6 activity

(A-D) S- and CH-CRs migration (Euclidean distance) in the 4 compartments: RM (A), CM (B), RL (C) and CL (D) for control and mutant cortices. Each point represents a cell.

(E) Control and mutant cortices were subdivided in 2 sections along the medial-lateral axis and in 3 sections along the rostro-caudal axis. In the 4 select compartments, mean displacement vectors were calculated from CR cell tracks. Vectors represent the Euclidean distance travelled during 8 hrs of migration.

Values shown are mean ± SEM; Anova test, *ns* not statistically different, $^{*}p<0.05$, $^{***}p < 0.001$.

Figure 4: Blocking extracellular Pax6 affects CR cell depth

(A, B) Position of S- (A) and CH-CR (B) neurons in the depth axis (Z) for control and mutant cortices, separated by compartment at the onset of tracking (RM, RL, CM and CL). For each cortex, values were weighted for comparison and are represented by percentage. This percentage does not represent the depth in a developing cortex *in vivo* as the VZ shrinks in culture because of the flattening. CRs localization was illustrated by representative S- and CH-CRs in each condition.

Values shown are mean ± SEM; Anova test, *ns*, not statistically different, $*p<0.05$, $**p< 0.01$, $***p< 0.001$.

Figure 5: Pax6 neutralization stimulates or inhibits CR cells undergoing contact-repulsion in a regions-dependent manner

(A) S- and CH-CR cells were clustered by: *contact*, if a CR cell encounters another CR cell during migration; *no contact* if a CR cell migrates without contacting another GFP^+ positive cell.

(B-D) Contact between two cells was subdivided in two categories: (B) *contact-repulsion* when contact with another CR cell resulted in the full retraction of their leading process, re-extension of a new leading process and change of initial direction (images taken from control CH-CR cells, blue circle); (C) *contact-without-repulsion* when contact with another CR cell did not change the direction (images taken from mutant S-CR cells, grey circle). Tracks are color coded for speed of migration . Directionality of migration was represented by a white arrow. (D) Quantification of contact-repulsion (filled bars) and contact-without-repulsion (hatched bars) of S- and CH-CR cells in control and mutant cortices.

Values shown are mean ± SEM; Anova test, *ns*, not statistically different, $*p<0.05$, $***p< 0.001$. Scale bar : 30 µm

Figure 6 : Pax6 modulates CR cell migration patterns through Ephrin A3

(A) Detail of a protein stripe assay in which Ephrin A3-containing stripes (green) alternate with laminin stripes (black). Hem-derived CR cells are labelled with DiAsP (red).

(B) Quantification of the distribution of cells along Ephrin A3-containing stripes versus laminin stripes.

Values shown are mean ± SEM; Anova test, *p<0.05, ***p< 0.001. Scale bar : 20 µm

Figure S1: Migration trajectories and speed at different time points

(A) Trajectories of S- and CH-CR cells at different time points. A theoretical starting point was taken and all cells from the 8 cortices (4 control and 4 mutant cortices) were pooled.

(B) Average speed of S- and CH-CR cells in controls and mutants after 480 min of recording. All cells from the 8 cortices were analyzed.

Values shown are mean ± SEM; Anova test, *ns* not statistically different..

Figure S2: Analysis of migration speed of S- and CH-CRs (related to figure 5)

Speed of S- (A) and CH-CR (B) cells in controls and mutants were evaluated at different time points. All cells from the 8 cortices were analyzed.

Values shown are mean ± SEM; Anova test, *ns* not statistically different, *p<0.05, **p< 0.01, ***p< 0.001.

References

Barber, M., Arai, Y., Morishita, Y., Vigier, L., Causeret, F., Borello, U., Ledonne, F., Coppola, E., Contremoulins, V., Pfrieger, F. W. et al. (2015) 'Migration Speed of Cajal-Retzius Cells Modulated by Vesicular Trafficking Controls the Size of Higher-Order Cortical Areas', *Curr Biol* 25(19): 2466-78.

Bernard, C., Vincent, C., Testa, D., Bertini, E., Ribot, J., Di Nardo, A. A., Volovitch, M. and Prochiantz, A. (2016) 'A Mouse Model for Conditional Secretion of Specific Single-Chain Antibodies Provides Genetic Evidence for Regulation of Cortical Plasticity by a Non-cell Autonomous Homeoprotein Transcription Factor', *PLoS Genet* 12(5): e1006035.

Bielle, F., Griveau, A., Narboux-Neme, N., Vigneau, S., Sigrist, M., Arber, S., Wassef, M. and Pierani, A. (2005) 'Multiple origins of Cajal-Retzius cells at the borders of the developing pallium', *Nat Neurosci* 8(8): 1002-12.

Borrell, V. and Marin, O. (2006) 'Meninges control tangential migration of hem-derived Cajal-Retzius cells via CXCL12/CXCR4 signaling', *Nat Neurosci* 9(10): 1284-93.

Brunet, I., Di Nardo, A. A., Sonnier, L., Beurdeley, M. and Prochiantz, A. (2007) 'The topological role of homeoproteins in the developing central nervous system', *Trends Neurosci* 30(6): 260-7.

Brunet, I., Weinl, C., Piper, M., Trembleau, A., Volovitch, M., Harris, W., Prochiantz, A. and Holt, C. (2005) 'The transcription factor Engrailed-2 guides retinal axons', *Nature* 438(7064): 94-8.

Ceci, M. L., Lopez-Mascaraque, L. and de Carlos, J. A. (2010) 'The influence of the environment on Cajal-Retzius cell migration', *Cereb Cortex* 20(10): 2348-60.

Di Lullo, E., Haton, C., Le Poupon, C., Volovitch, M., Joliot, A., Thomas, J. L. and Prochiantz, A. (2011) 'Paracrine Pax6 activity regulates oligodendrocyte precursor cell migration in the chick embryonic neural tube', *Development* 138(22): 4991-5001.

Griveau, A., Borello, U., Causeret, F., Tissir, F., Boggetto, N., Karaz, S. and Pierani, A. (2010) 'A novel role for Dbx1-derived Cajal-Retzius cells in early regionalization of the cerebral cortical neuroepithelium', *PLoS Biol* 8(7): e1000440.

Joliot, A. and Prochiantz, A. (2004) 'Transduction peptides: from technology to physiology', *Nat Cell Biol* 6(3): 189-96.

Knoll, B., Weinl, C., Nordheim, A. and Bonhoeffer, F. (2007) 'Stripe assay to examine axonal guidance and cell migration', *Nat Protoc* 2(5): 1216-24.

Lesaffre, B., Joliot, A., Prochiantz, A. and Volovitch, M. (2007) 'Direct non-cell autonomous Pax6 activity regulates eye development in the zebrafish', *Neural Dev* 2: 2.

Marin-Padilla, M. (1998) 'Cajal-Retzius cells and the development of the neocortex', *Trends Neurosci* 21(2): 64-71.

Matsuo, T., Osumi-Yamashita, N., Noji, S., Ohuchi, H., Koyama, E., Myokai, F., Matsuo, N., Taniguchi, S., Doi, H., Iseki, S. et al. (1993) 'A mutation in the Pax-6 gene in rat small eye is associated with impaired migration of midbrain crest cells', *Nat Genet* 3(4): 299-304.

Nomura, T., Holmberg, J., Frisen, J. and Osumi, N. (2006) 'Pax6-dependent boundary defines alignment of migrating olfactory cortex neurons via the repulsive activity of ephrin A5', *Development* 133(7): 1335-45.

O'Leary, D. D., Chou, S. J. and Sahara, S. (2007) 'Area patterning of the mammalian cortex', *Neuron* 56(2): 252-69.

Prochiantz, A. (2000) 'Messenger proteins: homeoproteins, TAT and others', *Curr Opin Cell Biol* 12(4): 400-6.

Prochiantz, A. and Di Nardo, A. A. (2015) 'Homeoprotein signaling in the developing and adult nervous system', *Neuron* 85(5): 911-25.

Stoykova, A., Hatano, O., Gruss, P. and Gotz, M. (2003) 'Increase in reelin-positive cells in the marginal zone of Pax6 mutant mouse cortex', *Cereb Cortex* 13(6): 560-71.

Tissir, F., Ravni, A., Achouri, Y., Riethmacher, D., Meyer, G. and Goffinet, A. M. (2009) 'DeltaNp73 regulates neuronal survival in vivo', *Proc Natl Acad Sci U S A* 106(39): 16871-6.

Villar-Cervino, V., Barreiro-Iglesias, A., Fernandez-Lopez, B., Mazan, S., Rodicio, M. C. and Anadon, R. (2013a) 'Glutamatergic neuronal populations in the brainstem of the sea lamprey, Petromyzon marinus: an in situ hybridization and immunocytochemical study', *J Comp Neurol* 521(3): 522-57.

Villar-Cervino, V., Molano-Mazon, M., Catchpole, T., Valdeolmillos, M., Henkemeyer, M., Martinez, L. M., Borrell, V. and Marin, O. (2013b) 'Contact repulsion controls the dispersion and final distribution of Cajal-Retzius cells', *Neuron* 77(3): 457-71.

Wizenmann, A., Brunet, I., Lam, J., Sonnier, L., Beurdeley, M., Zarbalis, K., Weisenhorn-Vogt, D., Weinl, C., Dwivedy, A., Joliot, A. et al. (2009) 'Extracellular Engrailed participates in the topographic guidance of retinal axons in vivo', *Neuron* 64(3): 355-366.

Yoshida, M., Assimacopoulos, S., Jones, K. R. and Grove, E. A. (2006) 'Massive loss of Cajal-Retzius cells does not disrupt neocortical layer order', *Development* 133(3): 537-45.

Ypsilanti, A. R. and Rubenstein, J. L. (2016) 'Transcriptional and epigenetic mechanisms of early cortical development: An examination of how Pax6 coordinates cortical development', *J Comp Neurol* 524(3): 609-29.

Figure 1

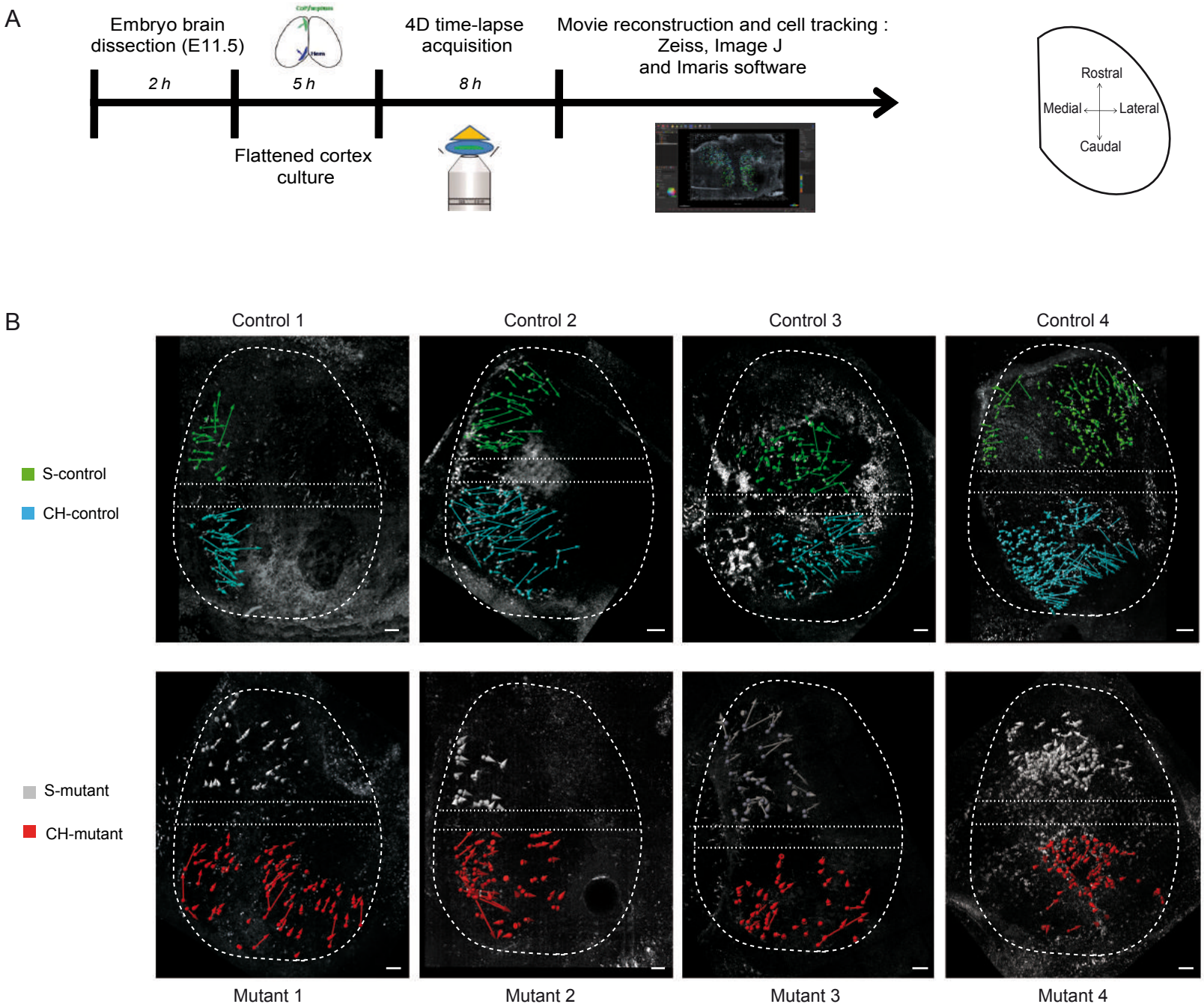
A
Embryo brain dissection (E11.5)
2 h
5 h
Flattened cortex culture
4D time-lapse acquisition
8 h
Movie reconstruction and cell tracking : Zeiss, Image J and Imaris software
Rostral
Medial
Lateral
Caudal
B
Control 1
Control 2
Control 3
Control 4
S-control
CH-control
S-mutant
CH-mutant
Mutant 1
Mutant 2
Mutant 3
Mutant 4

Figure 2

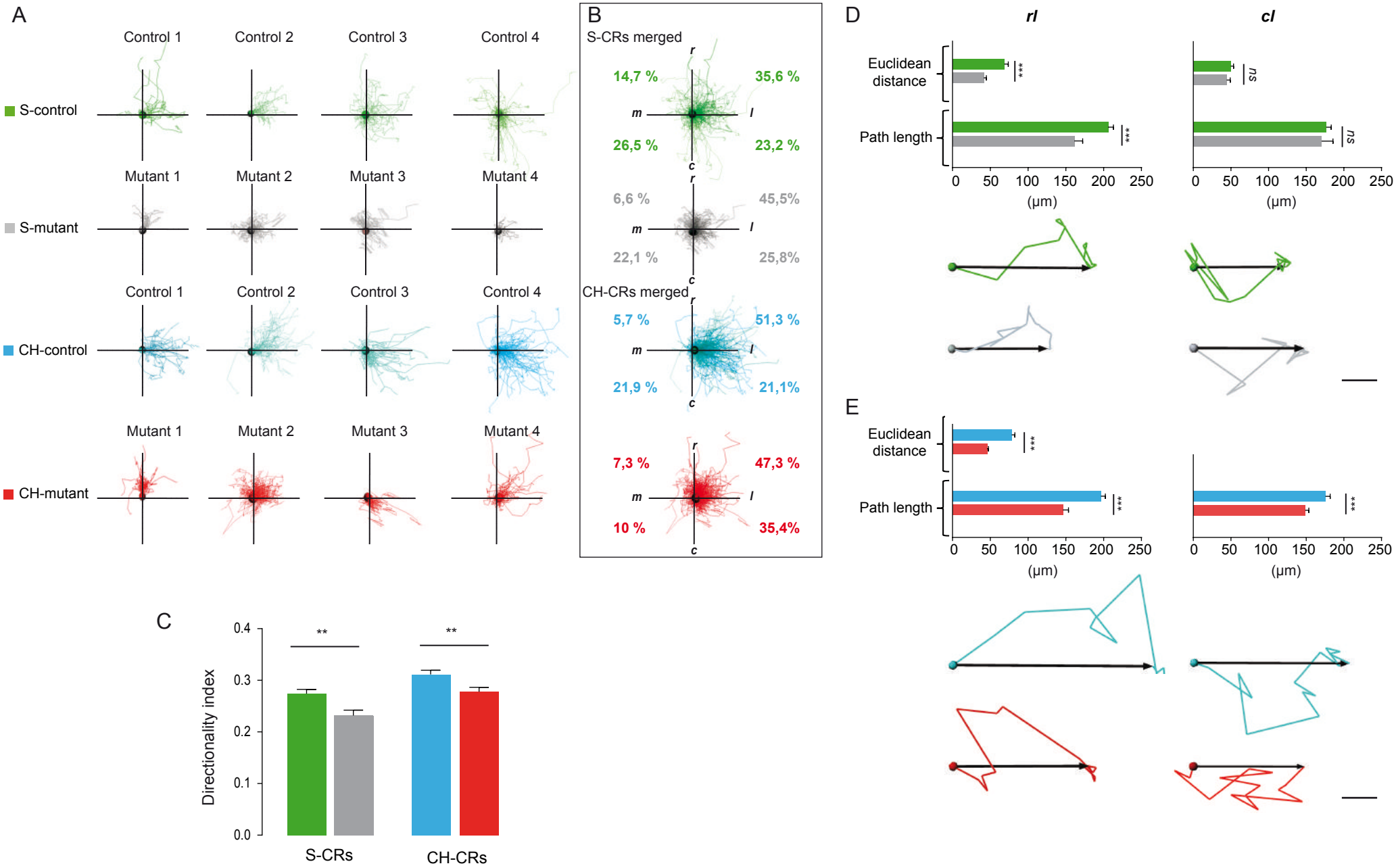
A
Control 1
Control 2
Control 3
Control 4
S-control
Mutant 1
Mutant 2
Mutant 3
Mutant 4
S-mutant
Control 1
Control 2
Control 3
Control 4
CH-control
Mutant 1
Mutant 2
Mutant 3
Mutant 4
CH-mutant
B
S-CRs merged
14,7 %
35,6 %
26,5 %
23,2 %
6,6 %
45,5%
22,1 %
25,8%
CH-CRs merged
5,7 %
51,3 %
21,9 %
21,1%
7,3 %
47,3 %
10 %
35,4%
r
l
m
c
C
Directionality index
0.4
0.3
0.2
0.1
0.0
**
**
S-CRs
CH-CRs
D
rl
cl
Euclidean distance
Path length
***
***
ns
ns
0
50
100
150
200
250
(µm)
E
Euclidean distance
Path length
***
***
***
0
50
100
150
200
250
(µm)

Figure 3

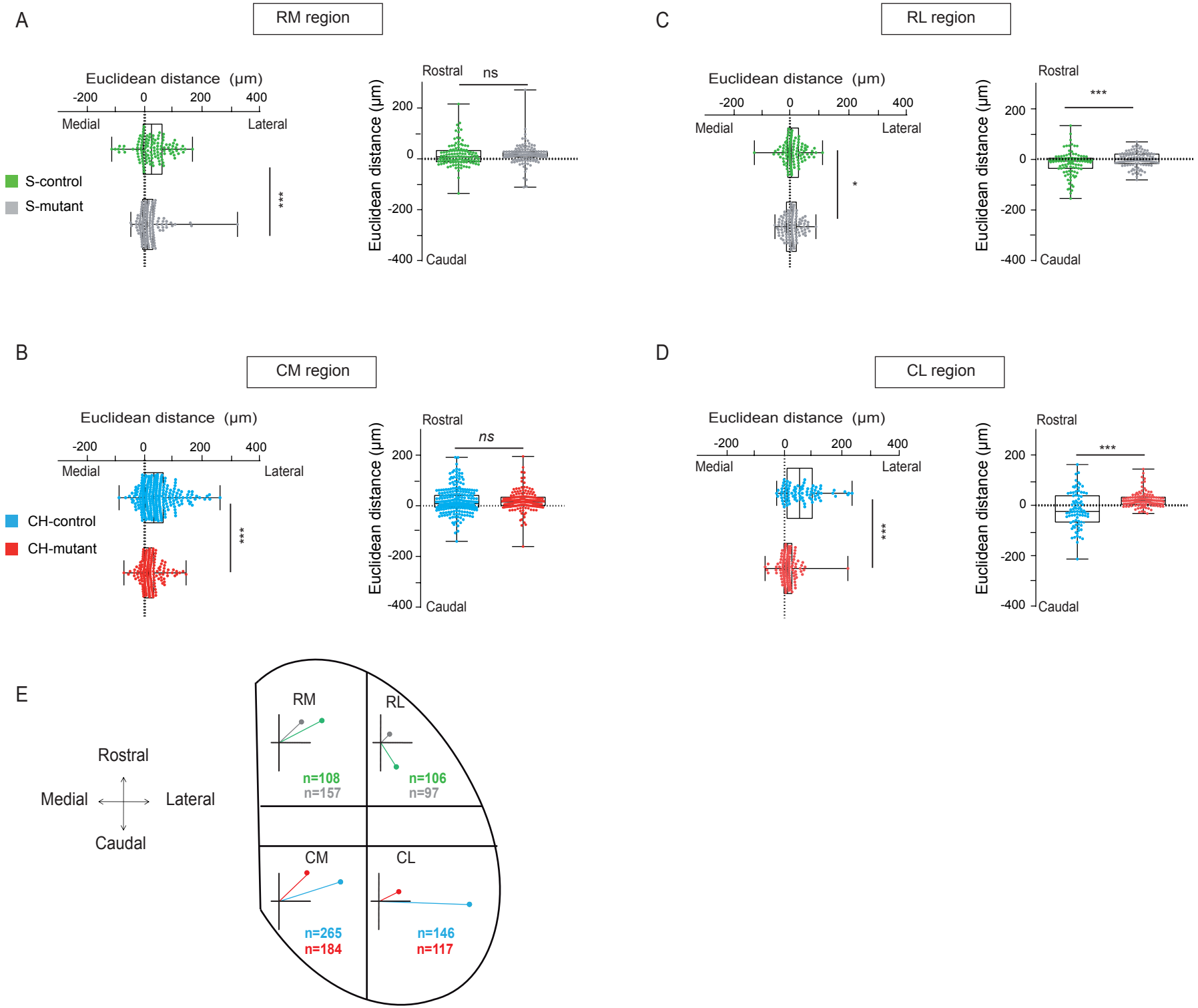
A
RM region
Euclidean distance (µm)
-200
0
200
400
Medial
Lateral
S-control
S-mutant
***
Rostral
ns
Euclidean distance (µm)
200
0
-200
-400
Caudal
C
RL region
Euclidean distance (µm)
-200
0
200
400
Medial
Lateral
*
Rostral
***
Euclidean distance (µm)
200
0
-200
-400
Caudal
B
CM region
Euclidean distance (µm)
-200
0
200
400
Medial
Lateral
CH-control
CH-mutant
***
Rostral
ns
Euclidean distance (µm)
200
0
-200
-400
Caudal
D
CL region
Euclidean distance (µm)
-200
0
200
400
Medial
Lateral
***
Rostral
***
Euclidean distance (µm)
200
0
-200
-400
Caudal
E
Rostral
Medial
Lateral
Caudal
RM
n=108
n=157
RL
n=106
n=97
CM
n=265
n=184
CL
n=146
n=117

Figure 4

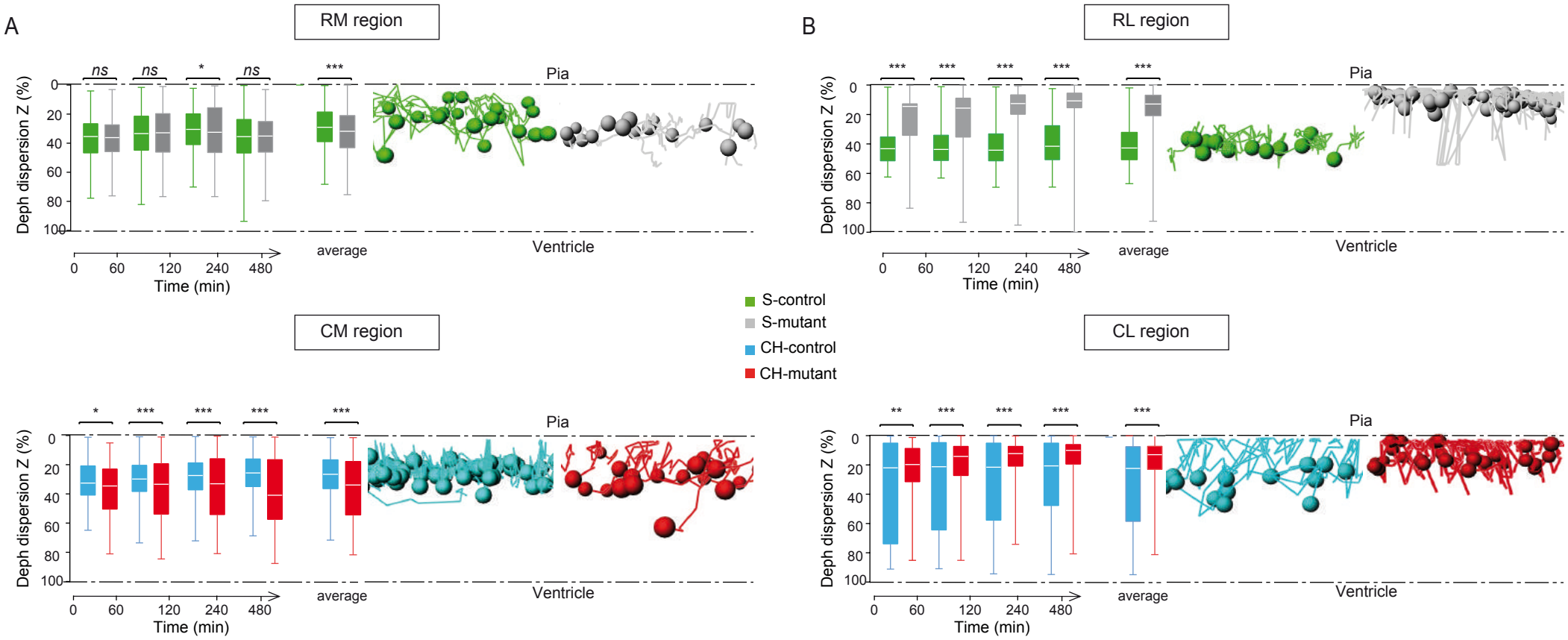
A
RM region
ns
ns
*
ns
***
Pia
Deph dispersion Z (%)
0
20
40
60
80
100
0
60
120
240
480
Time (min)
average
Ventricle
B
RL region
***
***
***
***
***
Pia
Deph dispersion Z (%)
0
20
40
60
80
100
0
60
120
240
480
Time (min)
average
Ventricle
S-control
S-mutant
CH-control
CH-mutant
CM region
*
***
***
***
***
Pia
Deph dispersion Z (%)
0
20
40
60
80
100
0
60
120
240
480
Time (min)
average
Ventricle
CL region
**
***
***
***
***
Pia
Deph dispersion Z (%)
0
20
40
60
80
100
0
60
120
240
480
Time (min)
average
Ventricle

Figure 5

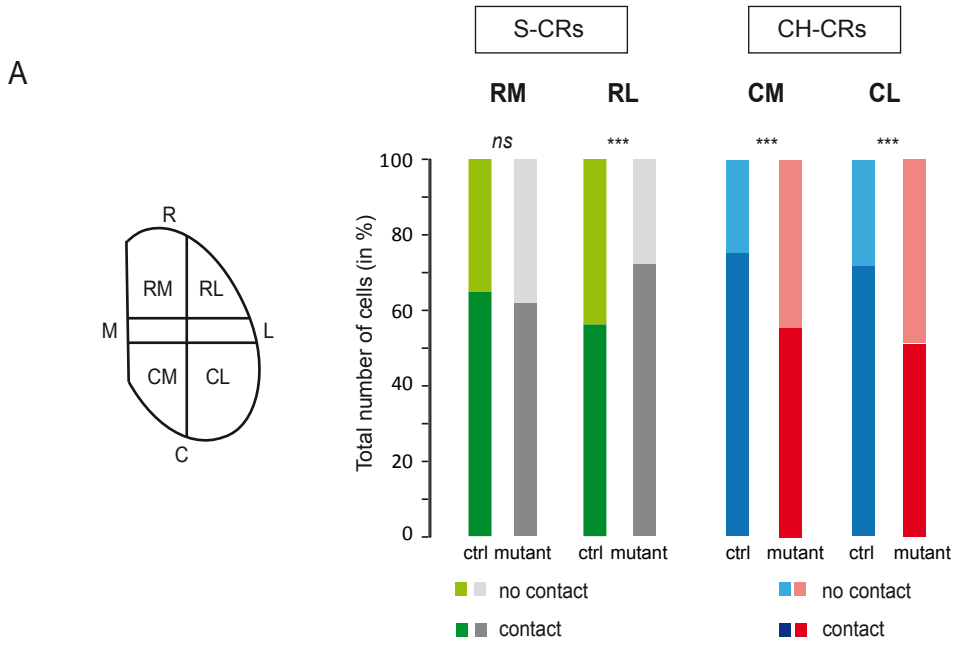
A
S-CRs
CH-CRs
RM
RL
CM
CL
ns
***
R
M
L
C
Total number of cells (in %)
100
80
60
40
20
0
ctrl mutant
no contact
contact

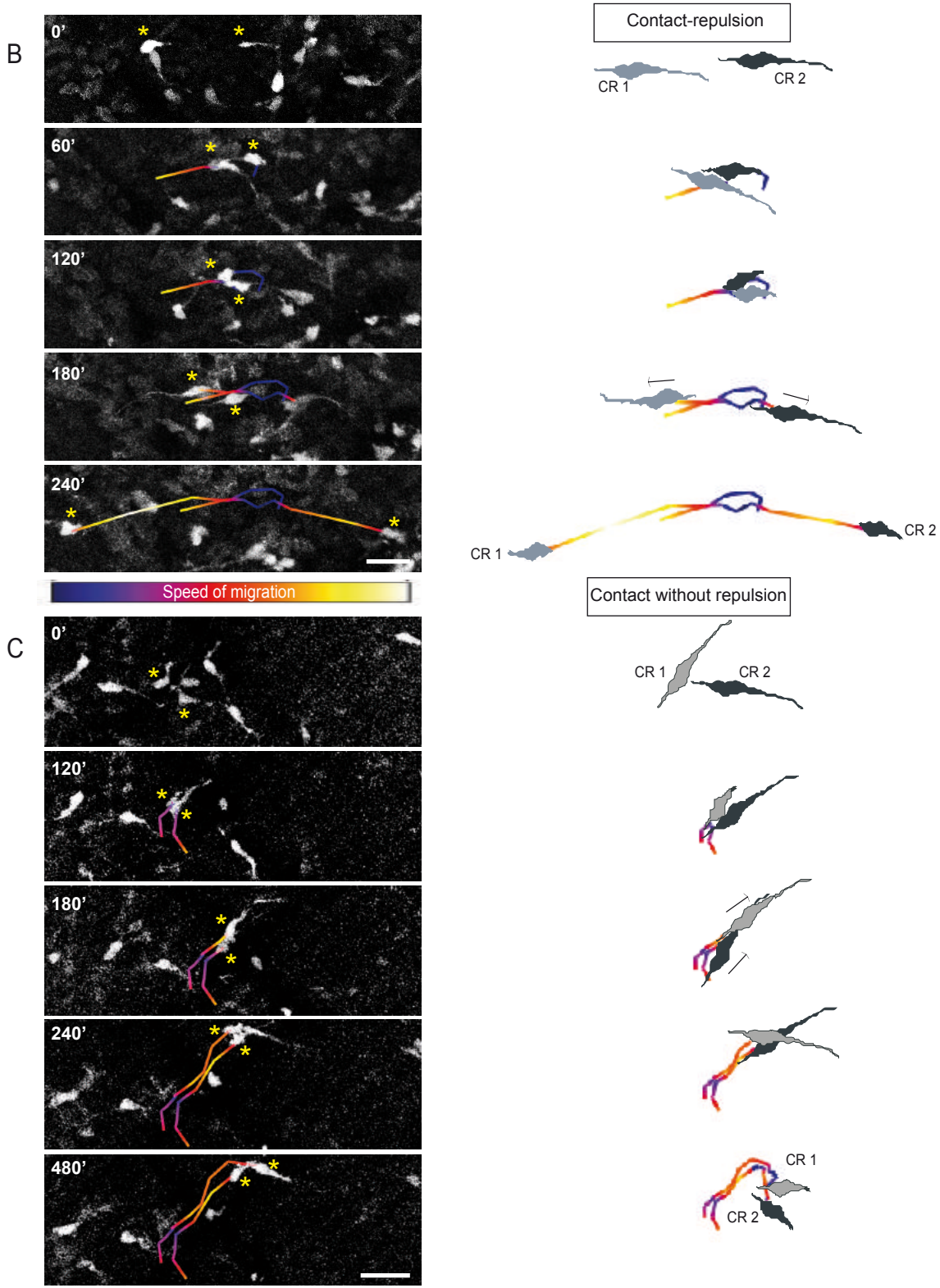
B
0'
60'
120'
180'
240'
Speed of migration
Contact-repulsion
CR 1
CR 2
C
0'
120'
180'
240'
480'
Contact without repulsion
CR 1
CR 2

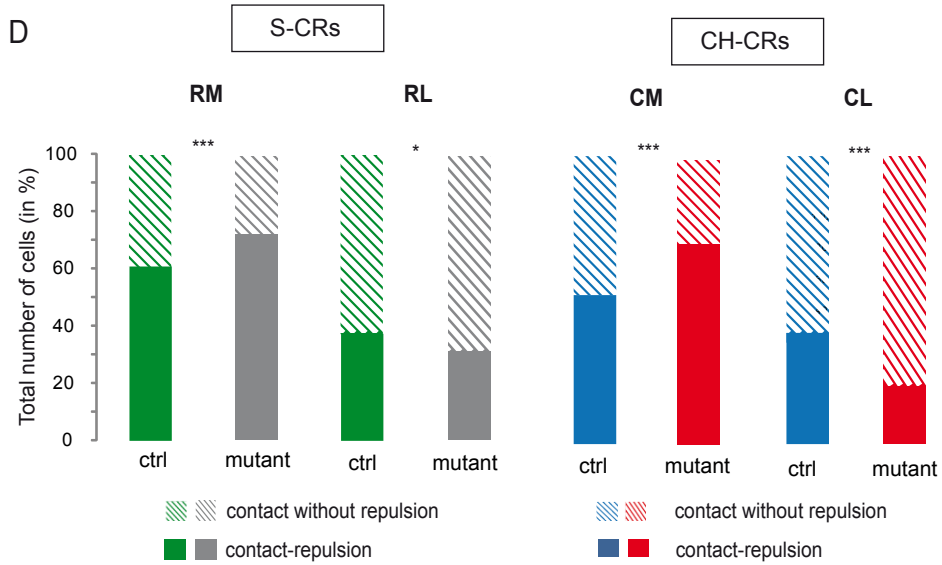
D
S-CRs
CH-CRs
RM
RL
CM
CL
***
*
Total number of cells (in %)
100
80
60
40
20
0
ctrl
mutant
contact without repulsion
contact-repulsion

Figure 6

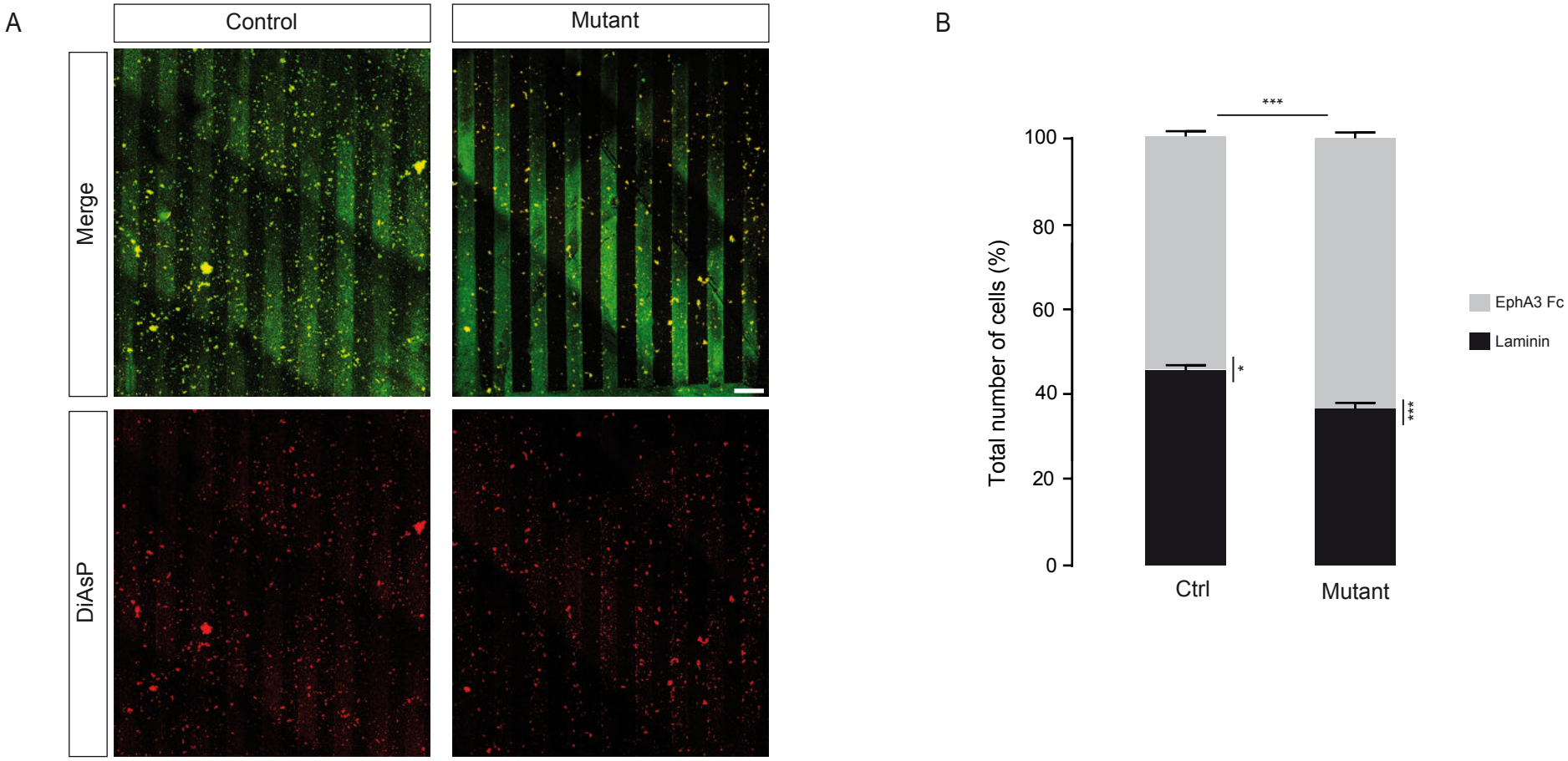
A
Control
Mutant
Merge
DiAsP
B
***
100
80
60
40
20
0
Total number of cells (%)
*
***
Ctrl
Mutant
EphA3 Fc
Laminin

Figure S1

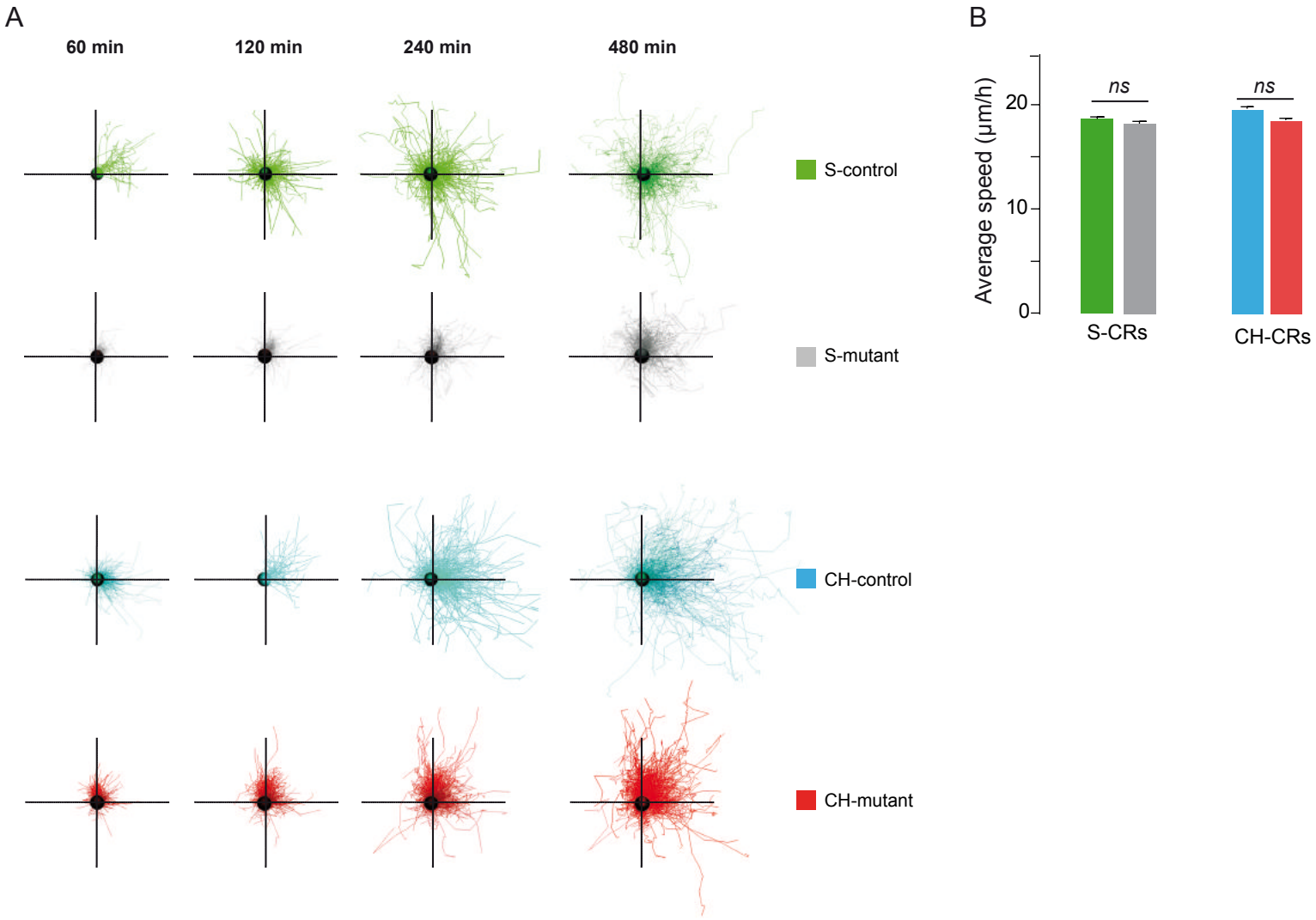
A
60 min
120 min
240 min
480 min
S-control
S-mutant
CH-control
CH-mutant
B
Average speed (µm/h)
20
10
0
ns
ns
S-CRs
CH-CRs

Figure S2

A

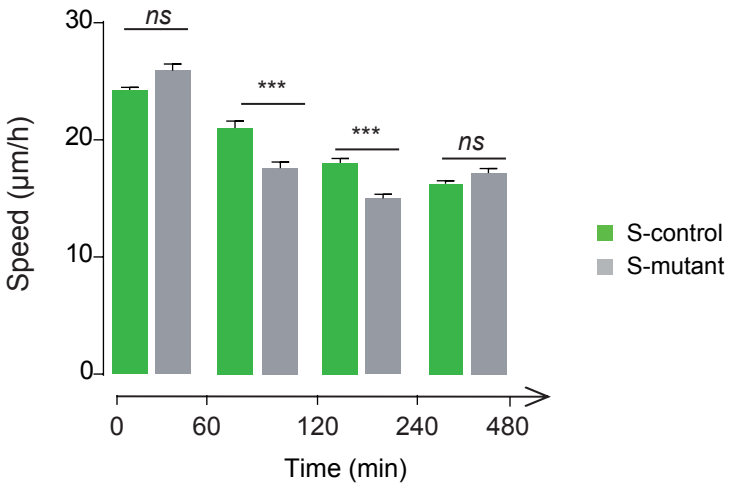
ns
***
***
ns
30
20
10
0
Speed (µm/h)
0
60
120
240
480
Time (min)
S-control
S-mutant

B

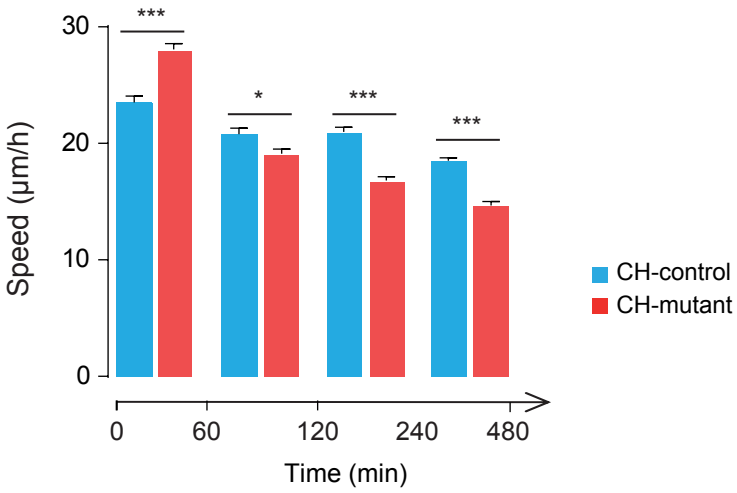
***
*
***
***
30
20
10
0
Speed (µm/h)
0
60
120
240
480
Time (min)
CH-control
CH-mutant